Electrochimica Acta 498 (2024) 144694

Contents lists available at ScienceDirect

Electrochimica Acta

journal homepage: www.journals.elsevier.com/electrochimica-acta

Unsupervised feature extraction for lithium-ion battery electrochemical impedance spectroscopy and capacity estimation using deep learning method

Jianying Yuan [a], Jie Zhao [a,*], Yaoguang Yu [b], Qingze Han [a], Guofeng Cui [c]

[a] School of Mechanical and Automotive Engineering, South China University of Technology, Guangzhou 510640, PR China
[b] School of Materials, Sun Yat-Sen University, Shenzhen 518107, PR China
[c] School of Chemistry, Sun Yat-Sen University, Guangzhou 510275, PR China

ARTICLE INFO

Keywords:
Capacity estimation
Electrochemical impedance spectroscopy
Lithium-ion battery
Unsupervised feature extraction
Variational autoencoder and generative adversarial network

ABSTRACT

In this paper, we propose an unsupervised feature extraction technique using a variational autoencoder and generative adversarial network (VAEGAN) that automatically extracts meaningful latent variables from the electrochemical impedance spectra (EIS) of lithium-ion (Li-ion) batteries. These variables accurately reflect the degree of Li-ion battery degradation and are closely related to its capacity. By analyzing the latent variables, it was found that the network can learn the effect of Li-ion battery capacity degradation on the EIS. The extracted latent variables are then used as input features for Gaussian Process Regression (GPR) to estimate the capacity of Li-ion batteries under uneven usage and with unknown historical data. The results show that the capacity prediction method proposed in this paper can significantly reduce prediction errors compared to the current state-of-the-art methods. The method not only provides a more reliable capacity estimation but is also robust to highly noisy EIS data, making it more suitable for practical application scenarios.

1. Introduction

The Li-ion battery has been widely used in energy storage systems, electric vehicles, and portable devices due to its high energy density, high power density, and low self-discharge rate [1,2]. As Li-ion batteries are utilized, they undergo irreversible reactions that decrease their capacity [3,4]. This capacity degradation is often accompanied by the degradation modes of conductivity loss (CL), loss of lithium inventory (LLI), and loss of active materials (LAM) [5,6]. Estimating Li-ion batteries' capacity with unknown aging levels is crucial for preventing battery failure and accidents. The degradation in capacity of Li-ion batteries is influenced by a multitude of factors [7], making the estimation of Li-ion battery capacity during aging a nontrivial task.

Data-driven capacity estimation methods have recently gained much attention due to the rapid development of machine learning and artificial intelligence [8,9]. Data-driven approaches can provide an accurate estimation of Li-ion battery aging state parameters when a certain amount of specific data collected by sensors is provided. This is in contrast to model-based methods, which rely on specific systems and require a greater amount of prior knowledge. The key to data-driven is feature engineering and the choice of modeling methods [10]. As it has been demonstrated that battery EIS has a close relationship with capacity degradation and can provide rich information about the dynamic characteristics of batteries over a wide frequency range [4,5,11], EIS data are the primary input features of choice for feature engineering in data-driven approaches. Compared to conventional techniques that rely on voltage, current, and temperature as input parameters, EIS offers more prompt and precise measurements of internal changes within batteries [12,13]. In addition, EIS is a non-destructive inspection method, and its measurements do not dramatically affect the battery, as well as reducing evaluation time.

Prior to utilizing EIS data to predict the aging state parameters of Li-ion batteries, it is of paramount importance to underscore the significance of data processing. This is commonly achieved through the subsequent approach: (1) Directly employ the raw impedance at all frequencies [14] (2). Figure out the impedance at the eigenfrequency that is strongly correlated with the parameter to be predicted [15–17] (3). Perform the equivalent circuit fitting to make predictions using the component parameters [17,18] (4). Perform the analysis of relaxation time distribution [19–21] (5). Geometrical characterization of the

* Corresponding author.
E-mail address: zhaoj77@scut.edu.cn (J. Zhao).

https://doi.org/10.1016/j.electacta.2024.144694
Received 7 May 2024; Received in revised form 18 June 2024; Accepted 8 July 2024
Available online 9 July 2024

Nyquist plots [22]. While all the aforementioned techniques can accurately predict the aging state parameters of Li-ion batteries, their widespread use is hindered by the requirement for substantial prior expertise and manual feature extraction performed by specialized personnel. With the rapid advancement of deep learning technology, neural networks can now be deployed to reduce data dimensions and extract intrinsic features of EIS [23–25]. This facilitates the prediction of the aging state of Li-ion batteries' parameters through automatic feature extraction, thereby eliminating the need for manual intervention. Additionally, it can be effectively employed for large-scale data processing, which represents a significant area for future advancement.

Numerous scholars have made progress in this research area, but there is still room for improvement. Zhang et al. [14] achieved the prediction of the state of health (SOH) and the remaining useful life (RUL) for Li-ion batteries by using only raw EIS data as input to GPR. This demonstrates the significant potential of EIS in battery management systems. Nevertheless, the direct prediction method using EIS data lacks robustness in addressing noise, necessitating enhanced processing of the input EIS. Obregon et al. [23] pre-trained a convolutional autoencoder (CAE) neural network to automatically encode the EIS data of Li-ion batteries. They subsequently implemented another neural network to predict the SOH. However, the features of interest extracted from EIS using CAE neural networks are discrete and lack clarity, making interpretation difficult. In addition, predicting the performance of Li-ion batteries based on the features suggested by the CAE neural network is vulnerable to the impact of noise in the EIS data. A more efficient feature extraction method for EIS data was proposed by Kim et al. [25]. They used Generative Adversarial Networks to extract additional explanatory latent variables from the EIS data of Li-ion batteries, leading to improved capacity estimation. However, designing suitable dimensions and types for coded variables is necessary and still poses a drawback. Additionally, the research is restricted to Li-ion batteries with a fixed cycling protocol, which significantly deviates from the actual usage of Li-ion batteries in practice. Jones et al. [26] proposed that EIS data, which reflects the cell response over various time scales, can serve as a state vector for the battery, thereby obviating the need to know the cycling history. As a result, performance forecasting for Li-ion batteries with uneven usage has been achieved. Ongoing research and enhancement are necessary for the reliable extraction of features related to the aging state parameters of Li-ion batteries from the EIS of Li-ion batteries undergoing uneven usage, and subsequently predicting their aging state parameters.

The VAEGAN model proposed in this paper, which is based on deep learning, can extract interpretable latent variables from the EIS data of Li-ion batteries in an unsupervised and automatic manner. By using the extracted latent variables as inputs to the GPR, it becomes feasible to estimate the capacity of Li-ion batteries that have undergone uneven usage during degradation. Using VAEGAN for feature extraction from EIS data has several advantages. Feature extraction is an unsupervised learning process. This means that during the feature extraction learning phase, unlabeled EIS data can be fully utilized. Second, automatic feature extraction can be achieved without any prior knowledge. Finally, its performance is robust to noise in EIS data. The proposed method is investigated using a publicly available database [26], in which the Li-ion batteries are subjected to uneven usage.

The remainder of the paper is organized as follows. The proposed VAEGAN model and the capacity estimation approach are described in Section 2. Data and implementation details are presented in Section 3. Section 4 examines the results of the GPR capacity estimation, as well as the latent variables discovered by VAEGAN. Section 5 concludes with a summary of the paper and provides recommendations for future research.

2. Methods

2.1. VAEGAN for unsupervised extraction of latent variables

VAEGAN is a model designed to derive significant latent variables from the EIS data of Li-ion batteries experiencing capacity degradation. The network structure of VAEGAN is illustrated in Fig. 1, wherein it is composed of a fusion of variational autoencoder (VAE) network and generative adversarial network (GAN). The generator is created to produce EIS data using latent variables in order to help understand these variables. The discriminator's goal is to differentiate between real and generated samples. The generator and discriminator play a key role in training the encoder to ensure it can extract significant and understandable latent variables from EIS data.

From a general probabilistic perspective, given a set of observations $\mathbf{X} = \{\boldsymbol{x}^{(1)}, \boldsymbol{x}^{(2)}, \ldots, \boldsymbol{x}^{(n)}\}$, where each $\boldsymbol{x}^{(i)}$ represents EIS data. Suppose that this set of observations is controlled by the latent variable $\mathbf{Z} = \{z^{(1)}, z^{(2)}, \ldots, z^{(n)}\}$, where $z^{(i)}$ is the latent variable corresponding to the ith EIS data. Finding the posterior probability $p_\theta(z|\boldsymbol{x})$ is necessary to figure out the latent variable $z^{(i)}$ that governs the observed sample $\boldsymbol{x}^{(i)}$. However, computing $p_\theta(z|\boldsymbol{x})$ typically involves integrating a function that is often challenging to integrate. According to the theory of variational inference [27], VAEGAN can approximate the posterior probability $p_\theta(z|\boldsymbol{x})$ by the distribution $q_\varphi(z|\boldsymbol{x})$ and evaluate the degree of approximation of the two distributions using the Kullback-Leibler (KL) divergence. The inference problem is effectively transformed into a simple optimization problem in the end. The computation of the KL divergence between the two distributions is expressed as follows:

$$D_{KL}(q_\varphi(z|\boldsymbol{x})\|p_\theta(z|\boldsymbol{x})) = E_{q_\varphi(z|\boldsymbol{x})}\left[\log\frac{q_\varphi(z|\boldsymbol{x})}{p_\theta(z|\boldsymbol{x})}\right] \tag{1}$$

Expanding $p_\theta(z|\boldsymbol{x})$ in Bayesian terms. Eq. (1) can be expressed in terms of the Evidence Lower Bound (ELBO).

$$D_{KL}(q_\varphi(z|\boldsymbol{x})\|p_\theta(z|\boldsymbol{x})) = -ELBO + \log p_\theta(\boldsymbol{x}) \tag{2}$$

$$ELBO = E_{q_\varphi(z|\boldsymbol{x})}[\log p_\theta(\boldsymbol{x}|z)] - D_{KL}(q_\varphi(z|\boldsymbol{x})\|\, p(z)) \tag{3}$$

For a given set of observed samples, the constant value of $\log p_\theta(\boldsymbol{x})$ shown in Eq. (2) converts the task of minimizing $D_{KL}(q_\varphi(z|\boldsymbol{x})\ \|p_\theta(z|\boldsymbol{x}))$ to maximizing the ELBO. The primary optimization aim of VAEGAN is to maximize the ELBO. In Eq. (3), the initial term on the right side of the equation indicates the level of similarity between the reconstructed sample and the original sample, while the second term signifies how closely the prior distribution $p(z)$ matches the distribution $q_\varphi(z|\boldsymbol{x})$, which is also referred to as the prior regularization. The encoder and generator of VAEGAN are required to enhance the ELBO by striking a balance between the reconstruction error and the prior regularization term. This equilibrium guarantees that the latent variables' distribution accurately converges to the posterior distribution $p_\theta(z|\boldsymbol{x})$.

The discriminator in VAEGAN can learn a rich measure of similarity to the data and is used to determine whether the input samples are from generated or actual samples. A prospective feature vector should typically be approximated if an input sample is close. Therefore, prospective features discovered by the discriminator are utilized to calculate the reconstruction error. As a result, the feature similarity learned by the discriminator network can replace the reconstruction error in ELBO. The output of the lth layer of the discriminator network is specifically denoted as $\mathrm{Dis_l}(\boldsymbol{x})$, and the equation below can be used to substitute the original reconstruction error of ELBO.

$$\mathscr{L}_{\mathrm{llike}}^{\mathrm{Dis_l}} = -E_{q_\varphi(z|\boldsymbol{x})}[\log p(\mathrm{Dis_l}(\boldsymbol{x})|z)] \tag{4}$$

2.2. GPR for capacity estimation

Using the Gaussian Process (GP) to characterize the probability

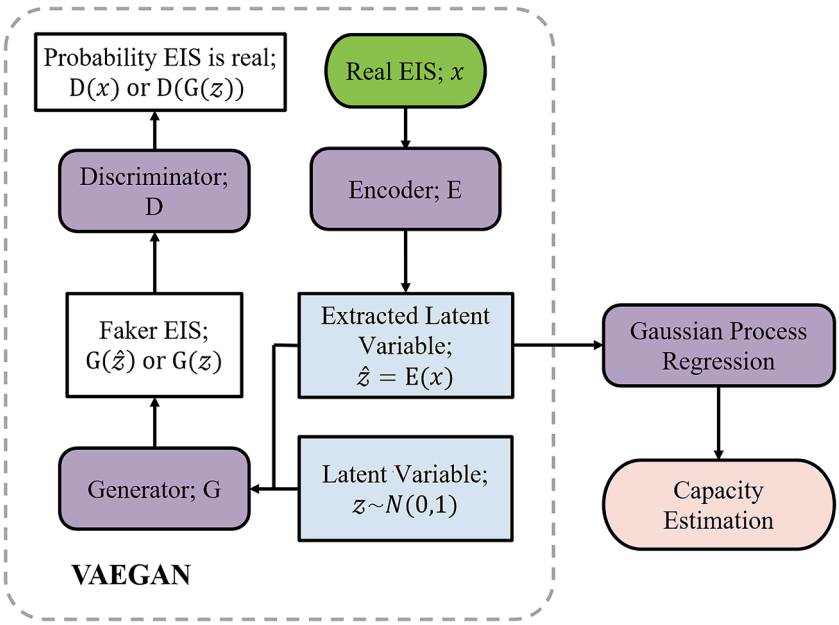

Fig. 1. Network structure of VAEGAN and procedure of capacity estimation using GPR.

distribution of a function for prediction and uncertainty estimates, GPR is a nonparametric regression technique based on Bayesian inference [28].

Given a dataset $D = \{(x^{(i)}, y^{(i)}) \mid i = 1, 2, \cdots, n\} = (\mathbf{Z}, \mathbf{Y})$, the GPR model relates the response to the inputs by:

$$y^{(i)} = f(x^{(i)}) + \xi^{(i)} \tag{5}$$

where $y^{(i)}$ is the capacity of the Li-ion battery, $x^{(i)}$ is a vector of latent variables extracted from the EIS data, and $\xi^{(i)} \sim N(0, \sigma_n^2)$ is the independent and identically distributed Gaussian noise. To simplify representation, it is common to assume that the GP has a mean function of zero and a covariance function of $k(x, x')$, at which $f(x) \sim GP(0, k(x, x'))$. The prior distribution of the output $\mathbf{Y}$ of the training samples is

$$\mathbf{Y} \sim N(0,\ \mathbf{K}(\mathbf{Z}, \mathbf{Z}) + \sigma_n^2 \mathbf{I}) \tag{6}$$

where I is the unit matrix, $\mathbf{K}(\mathbf{Z}, \mathbf{Z}) = (\mathrm{K_{ij}})$ is a symmetric positive definite covariance matrix of order $n \times n$ and the matrix element $\mathrm{K_{ij}} = k(x_\mathrm{i}, x_\mathrm{j})$ describes the correlation between x_i and x_j.

The joint Gaussian distribution is formed by the training sample output $\mathbf{Y}$ and the predicted value $\mathbf{Y}'$ of the new input sample $\mathbf{Z}'$ as:

$$\begin{bmatrix} \mathbf{Y} \\ \mathbf{Y}' \end{bmatrix} \sim N\left(0, \begin{bmatrix} \mathbf{K}(\mathbf{Z}, \mathbf{Z}) + \sigma_n^2 I & \mathbf{K}(\mathbf{Z}, \mathbf{Z}') \\ \mathbf{K}(\mathbf{Z}', \mathbf{Z}) & \mathbf{K}(\mathbf{Z}', \mathbf{Z}') \end{bmatrix}\right) \tag{7}$$

where $\mathbf{K}(\mathbf{Z}, \mathbf{Z})$ is the self-covariance matrix of the training sample $\mathbf{Z}$, $\mathbf{K}(\mathbf{Z}, \mathbf{Z}') = \mathbf{K}(\mathbf{Z}', \mathbf{Z})$ is the covariance matrix of the training samples $\mathbf{Z}$ and test samples $\mathbf{Z}'$, and $\mathbf{K}(\mathbf{Z}', \mathbf{Z}')$ is the self-covariance matrix of the test sample $\mathbf{Z}'$. The parameters of the model are determined by maximizing the marginal log-likelihood function of the training dataset. According to the concept of a joint Gaussian distribution, the predicted value $\mathbf{Y}'$ can be calculated using the following formula.

$$\mathbf{Y}' | \mathbf{Z}, \mathbf{Y}, \mathbf{Z}' \sim N(\mu, \Sigma) \tag{8}$$

$$\mu = \mathbf{K}(\mathbf{Z}', \mathbf{Z}) \left[\mathbf{K}(\mathbf{Z}, \mathbf{Z}) + \sigma_n^2 \mathbf{I}\right]^{-1} \mathbf{Y} \tag{9}$$

$$\Sigma = \mathbf{K}(\mathbf{Z}', \mathbf{Z}') - \mathbf{K}(\mathbf{Z}', \mathbf{Z}) \left[\mathbf{K}(\mathbf{Z}, \mathbf{Z}) + \sigma_n^2 \mathbf{I}\right]^{-1} \mathbf{K}(\mathbf{Z}, \mathbf{Z}') \tag{10}$$

3. Experimental data and implementation

3.1. Experimental data

EIS data reported in the article [26], which tested commercially available 35-mAh PowerStream LiR2032 coin cells, are utilized to validate the approaches discussed in this study. The data used in this paper comes from batteries numbered PJ121–126 within the database. The charging and discharging processes, as well as the EIS measurements, were conducted at a temperature of 23 ± 2°C. For the charging procedure, it involves two stages of constant current (CC) charging. In Stage I, the current level is randomly chosen from between 70 and 140 mA (2C-4C), while in Stage II, the current level is randomly chosen from between 35 and 105 mA (1C-3C). Each stage's charging time was 15 min until the battery voltage reached the 4.3 V charging cut-off voltage. The battery was fully charged and allowed to rest for 20 min, and then the EIS data used in this article were measured with an excitation current of 5 mA and a frequency range of 0.02 Hz to 20 kHz. The battery capacity was determined by discharging the battery at a constant current of 52.5 mA (1.5 C) until the voltage reached 3.0 V at the end of each cycle. Fig. 2 shows the variation of the EIS measurements and capacity of one of several batteries used from cycle to cycle. The figure represents the real and imaginary parts of the impedance as Z' and Z'', respectively.

3.2. Data preprocessing

Pre-processing of the sample data is necessary to standardize the format of the input data and enhance the performance of the neural network [29]. Converting EIS data into matrices with specific dimensions and number of channels facilitates the input of complex networks like convolutional neural networks. This approach enables the neural network to focus on the relationships among data points as a whole rather than on the value of a single point. The benefits of this method have been verified in reference [23,30].

We use cubic spline interpolation to fit 57 impedance values at the original frequencies ranging from 0.02 Hz to 20 kHz and resample the EIS data with a length of 200. The impedance $Z(f)$ can be divided into its real part, $\mathrm{Re}(Z(f))$, and its imaginary part, $\mathrm{Im}(Z(f))$. $Z(f)$ can be expressed as $\mathrm{Re}(Z(f)) + j\mathrm{Im}(Z(f))$, where j is an imaginary unit. Finally, the single sample EIS data is converted into a matrix x with a channel

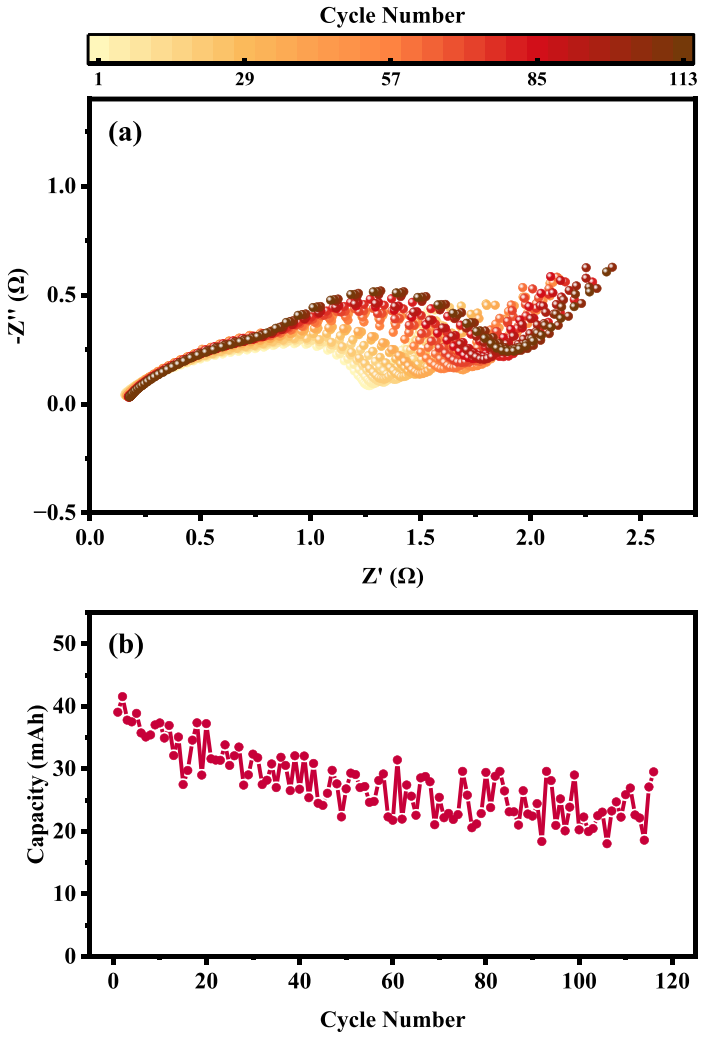

Fig. 2. The raw data of the PJ121 battery during the cycles. (a) EIS. (b) Capacity.

count of $C = 2$ and a length of $N = 200$ as follows:

$$x = \begin{bmatrix} \mathrm{Re}(Z(f_1)) & \mathrm{Re}(Z(f_2)) & \cdots & \mathrm{Re}(Z(f_n)) \\ \mathrm{Im}(Z(f_1)) & \mathrm{Im}(Z(f_2)) & \cdots & \mathrm{Im}(Z(f_n)) \end{bmatrix} \in \mathbb{R}^{C\times N} \tag{11}$$

The matrix x of the sample EIS data must undergo a Z-score normalization process after it has been transformed [31]. After calculating the mean matrix μ and the standard deviation matrix σ for each feature dimension of the training set samples, the following operations are performed on the dataset:

$$x' = (x-\mu)/\sigma \tag{12}$$

It should be noted that the mean and deviation are calculated using the training dataset rather than the entire sample, so when the training set is changed, the mean and deviation must be recalculated to account for it and perform the data's Z-score transformation, which is a special consideration in the K-fold Cross-Validation process.

Li-ion battery capacity estimation during capacity degradation based on VAEGAN and GPR using a six-fold cross-validation approach; that is, data from one battery from PJ121–126 batteries is chosen as the test set in turn, and data from the other five sets of batteries is used as the training set to validate the method in six rounds. The VAEGAN does not require a test set or a validation set as it utilizes an unsupervised learning technique that solely relies on the five battery data sets from the training set. GPR updates parameters using the training set and validates them using the test set.

3.3. Model implementation

3.3.1. VAEGAN

In this study, we construct a VAEGAN network using PyTorch. Fig. 3 illustrates the specific topology and training procedure of the network. The 1D Convolutional Layer and 1D Max-Pooling Layer are capable of extracting detailed feature information from the input data without neglecting the relationships between the input data as a whole. To enhance the network's learning capacity, prevent gradient vanishing, and expedite the model's convergence, one can strategically increase the number of layers in the network by incorporating the BatchNorm Layer and LeakyReLU activation functions [32]. The linear layer in VAEGAN is primarily used to modify feature dimensions and enable connections to the upper and lower layers.

The three primary data flow segments in the model are depicted in Fig. 3 through the orange, green, and blue lines. The orange line illustrates the initial step where the input data is encoded by the encoder to produce mean and variance vectors for the posterior distribution. Subsequently, the reparameterization technique [27] is applied to derive the latent variable, z. The generator then decodes this latent variable to reconstruct the input data. The reconstructed data, denoted as $\tilde{x}$, undergoes evaluation by the discriminator to yield latent vectors representing the potential characteristics of the input data. The blue line signifies the phase where the original input data is inputted into the discriminator for assessment, resulting in the generation of a latent vector reflecting the data's attributes. The reconstruction error can be

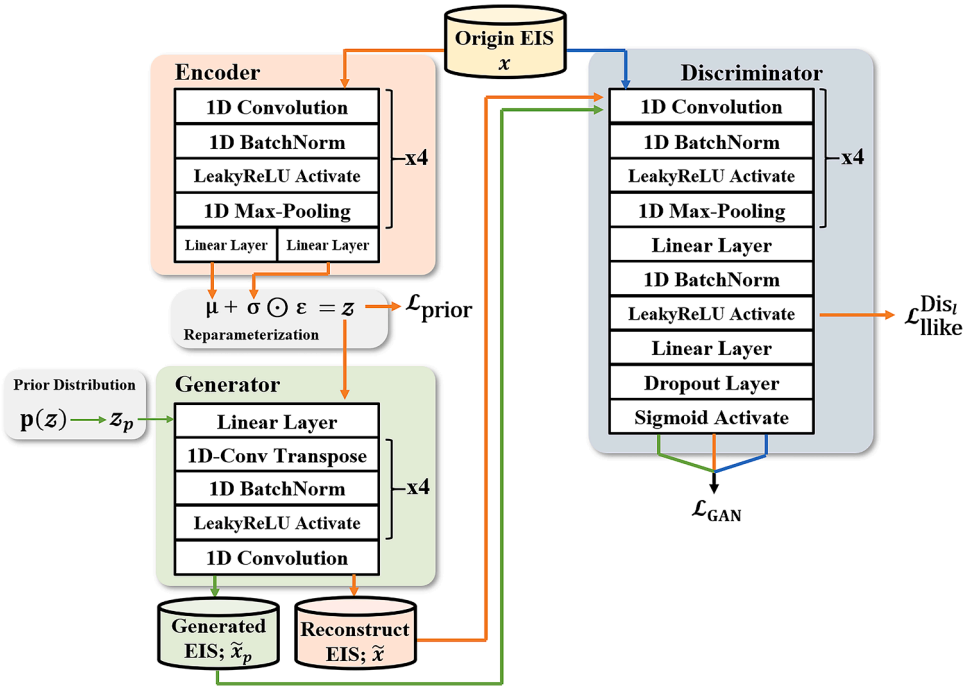

Fig. 3. The structure and training strategy of the proposed VAEGAN for unsupervised EIS data extraction. Arrows of various colors represent distinct training sessions.

computed by amalgamating the latent vectors of the reconstructed and original data acquired in the aforementioned steps. The green line illustrates the generation of "fake samples." This involves selecting random values of the latent variable z_p from the latent variable space, which are then inputted into the generator to produce the sample $\tilde{x}_p$. Subsequently, this sample is forwarded to the discriminator for authentication.

Three major components make up the loss of the VAEGAN neural network. The loss of the encoder is expressed as follows:

$$\mathcal{L}_{\text{Enc}} = \mathcal{L}_{\text{prior}} + \mathcal{L}_{\text{llike}}^{\text{Dis}_l} = D_{KL}(q_\varphi(z|x)\| p(z)) - E_{q_\varphi(z|x)}[\log p(\text{Dis}_l(x)|z)] \tag{13}$$

The discriminator assigns probability $y = \text{Dis}(x) \in [0, 1]$ to x being an actual training sample and probability $1 - y$ to $\tilde{x}$ or $\tilde{x}_p$ being created by our model. The objective of model training is to improve the discriminator's ability to distinguish between real and generated data, as well as to encourage the generator to generate data that matches closely the distribution of the real data. Thus, the losses of the generator and the discriminator can be expressed by the binary cross-entropy as follows, respectively.

$$\mathcal{L}_{\text{Gen}} = \mathcal{L}_{\text{llike}}^{\text{Dis}_l} - \log(\text{Dis}(\tilde{x})) - \log(\text{Dis}(\tilde{x}_p)) \tag{14}$$

$$\mathcal{L}_{\text{GAN}} = -\log(1 - \text{Dis}(\tilde{x})) - \log(1 - \text{Dis}(\tilde{x}_p)) - \log(\text{Dis}(x)) \tag{15}$$

The VAEGAN training procedure optimizes model parameters using the AdamP optimizer. The learning rates for the encoder, generator, and discriminator are set to 0.01, 0.005, and 0.005, respectively.

3.3.2. GPR

The capacity of Li-ion batteries is estimated using GPR as a benchmark approach to demonstrate the ability of the VAEGAN model in this paper to learn and extract characteristics from raw EIS data.

The input z to the GPR is of the following form:

$$z = \left[z^{(1)}, z^{(2)}, \cdots, z^{(n)}\right]^T \tag{16}$$

where $z^{(i)} = (z_1, z_2)$ is a vector of latent variables extracted by the encoder in VAEGAN from the ith input sample. The length of the latent variable vector in this paper is set to be ten. Before the VAEGAN training, the training set and the test set were already partitioned.

The mean function of the Gaussian process is set to 0 in this article, and the squared exponential kernel function is used as the covariance kernel function. GPR is trained by updating the model parameters with the training dataset in order to optimize the marginal log-likelihood function. The GPML toolbox is used to implement GPR in Matlab [33]. The mean and confidence interval of the Li-ion battery capacity prediction y_{test} are determined using Eqs. (8)–(10) at the end of training.

3.3.3. Evaluation metrics

Since estimating capacity during Li-ion battery capacity degradation is a regression issue, this study evaluates and compares model performance using two commonly used metrics: root mean square error (RMSE) and mean absolute error (MAE).

$$RMSE = \sqrt{\frac{\sum_{i=1}^{n}(y_i - \hat{y}_i)^2}{n}} \tag{17}$$

$$MAE = \frac{\sum_{i=1}^{n}|y_i - \hat{y}_i|}{n} \tag{18}$$

$\hat{y}_i$ and y_i denote the predicted and actual measured capacity values for the ith cycle, respectively, and n is the number of test samples.

4. Results and discussion

4.1. Generation of reliable EIS data

In the fields of statistics and machine learning, a latent variable refers to a variable that is not directly observable but plays a role in explaining or influencing observable samples. Within the VAEGAN framework, the latent variable z is characterized as a low-dimensional continuous vector that captures essential characteristics of the EIS data. The validity of a latent variable within a model can be assessed by evaluating the model's ability to produce consistent EIS data using the latent variable. In the

VAEGAN model, the generator is capable of producing reliable EIS data by utilizing latent variable vectors obtained through sampling from the prior distribution of the latent variables, denoted as $p(z)$.

During model training, the prior distribution of the latent variables is assumed to follow a Gaussian distribution. Therefore, the range of real values [−2, 2] represents the 95 % confidence intervals of the latent variable distribution. The following approach can be used to generate new EIS data, x_g:

$$x_g = Gen(z), \quad -2 \le z \le 2 \tag{19}$$

In the VAEGAN model, the encoder extracts ten latent variables, with z_1 and z_2 being particularly relevant to the variations in Li-ion battery cycle capacities. To create the latent variable vectors, one of these variables, z_1 or z_2, is chosen to follow a uniform distribution between −2 and 2, while the other latent variables are set to zero. These vectors are intended to facilitate the generation of electrochemical impedance spectroscopy (EIS) data by the VAEGAN generator. The resulting data is presented in Fig. 4. The figure demonstrates that a decrease in the value of z_1 leads to an increased prominence of the first semicircle in the generated EIS, accompanied by a rightward shift of the second semicircle. Conversely, an increase in the value of z_2 results in the enlargement of both semicircles in the generated EIS, with a particularly noticeable change observed in the second semicircle.

To investigate the correlation between the latent variables extracted from VAEGAN and the degradation of Li-ion batteries' capacity, the EIS generated by the latent variables is fitted to a suitable equivalent circuit model [34]. With the help of analyzing the variation of component parameters in the equivalent circuit, the extracted latent variables are related to the degradation mechanism of the Li-ion battery. The equivalent circuit for EIS fitting is depicted in Fig. 5(a): a resistor, two ZARC elements [35], and constant phase element (CPE) components connected in series. The R_S represents the electrolyte resistance of the Li-ion battery and the contact resistance of the electrodes. The two ZARC elements represent the Li-ion battery's solid electrolyte interface (SEI) layer and the charge transfer process, respectively. The CPE_W represents the non-ideal diffusion behavior of the electrode surface. The fitting result of the equivalent circuit model for the EIS is shown in Fig. 5(b).

The relationship between the variation of latent variables and the variation of the parameters of the equivalent circuit elements can be established by fitting the generated EIS to the equivalent circuit and extracting the parameters from it. Fig. 5(c, d) demonstrates that the fluctuations in the latent variables are highly correlated with the components in the equivalent circuit, specifically R_{SEI}, R_{ct}, and CPE_W. The only relationship between the z_1 and R_{ct} suggests that any change in the

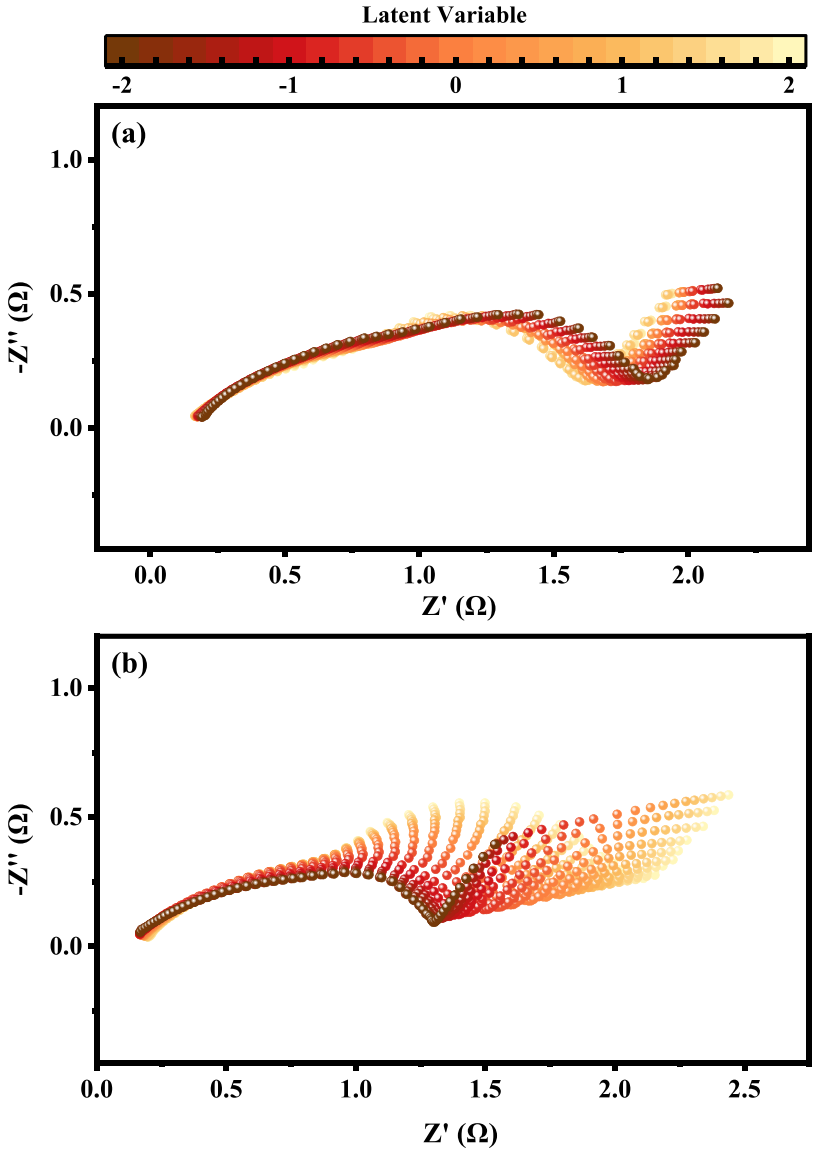

Fig. 4. The EIS data is generated through latent variables. (a) z_1 and (b) z_2.

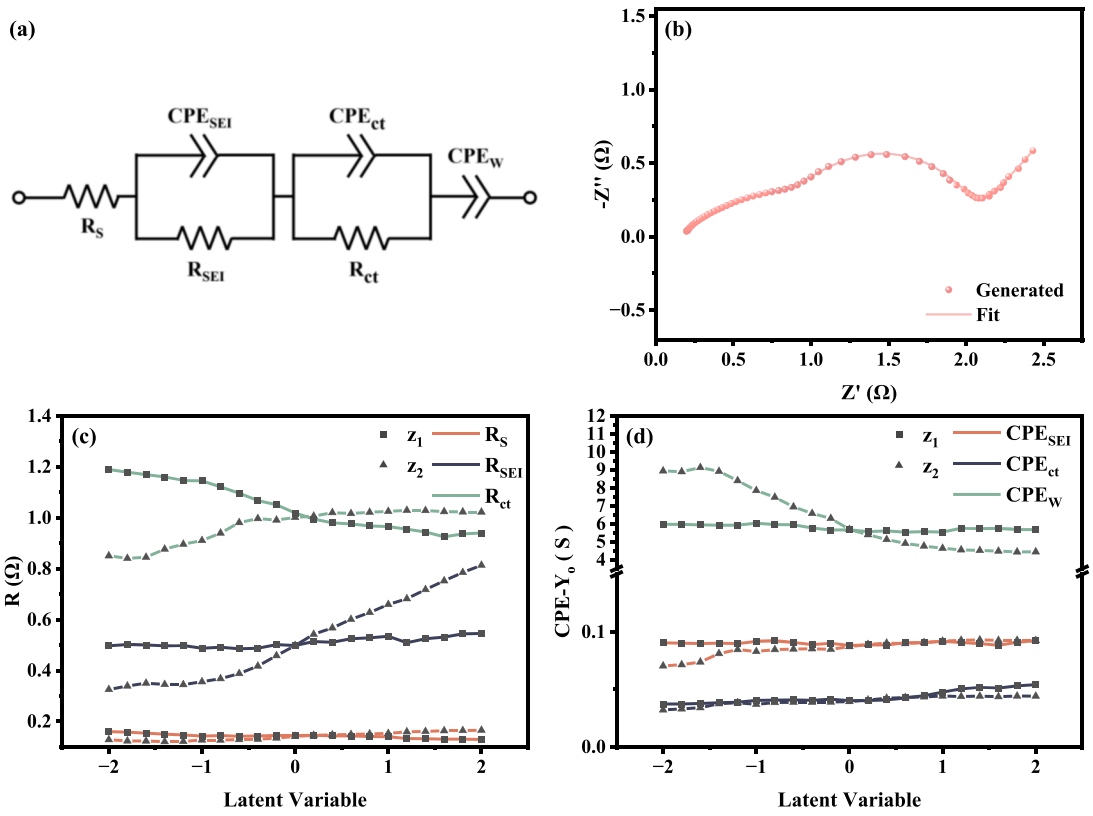

Fig. 5. Equivalent circuit model and trend of its components with latent variables. (a) Equivalent circuit. (b) EIS fitting situation. (c) Resistance and (d) conductivity of CPE vary with latent variables.

z_1 solely reflects the charge transfer process of the Li-ion battery. The difficulty of charge transfer increases as the decreasing z_1. This decrease indicates the occurrence of degradation mechanisms such as Li plating, structural decomposition of the cathode, and particle cracking. With the increase of z_2, both R_{SEI} and R_{ct} tend to increase. This indicates that the charge transfer process becomes more challenging due to the decrease in lithium-ion concentration caused by SEI growth [36,37]. The changes in R_{SEI} and R_{ct} correspond to the LLI and LAM of Li-ion batteries, respectively. The conductance of the CPE_W decreases as z_2 increases. It is often associated with phenomena that occur on the electrodes of Li-ion batteries, such as structural decomposition and particle fracture. It should be assigned to the LAM of Li-ion batteries [38].

In conclusion, by utilizing the EIS data from long-term used Li-ion batteries, the VAEGAN is capable of learning the EIS trend associated with the capacity deterioration of Li-ion batteries caused by LLI and LAM. Furthermore, it can accurately quantify and describe this trend of EIS using latent variables.

4.2. Extraction of latent variables from the EIS

Fig. 6 shows the latent variables z_1 and z_2, which were obtained by the encoder of VAEGAN from the EIS data of PJ121–126 batteries as the cycles increased. The latent variables that VAEGAN extracts from the input EIS will contain a certain amount of random noise, this is because the encoder of VAEGAN maps the input EIS data to a distribution of latent variables rather than an exact value. It is particularly evident in the latent variable z_2 that the magnitude of the noise variance increases as the number of cycles increases. This indicates that the uncertainty of the latent variable also increases with the number of cycles. The latent variable z_1 exhibits a monotonically declining trend followed by a monotonically growing trend, while z_2 effectively grows monotonically with the number of loops. As described in Section 4.1, z_1 is only associated with the size of the first semicircular arc of the EIS. On the other hand, z_2 is associated with the size of both the first and second arcs. Additionally, the rate of change of the second arc size remains relatively constant as the number of cycles of the Li-ion battery increases. In

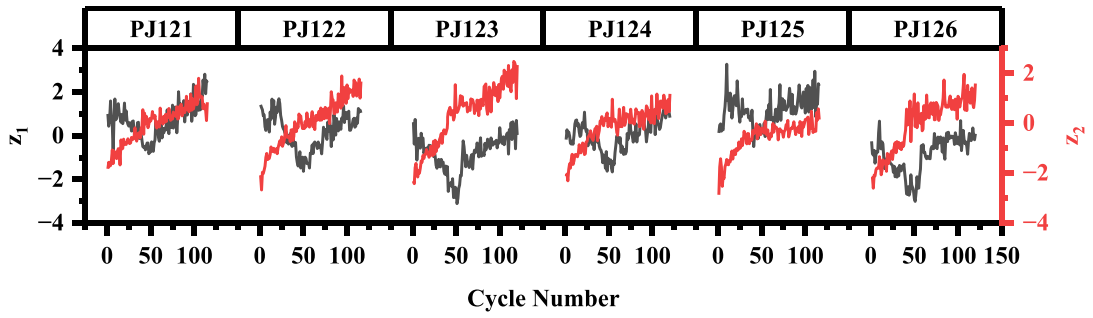

Fig. 6. Extracted latent variables z_1 and z_2 from PJ121–126. The latent variables are selected based on the correlation with the capacity and arranged in decreasing order with the cycles.

contrast, the rate of change of the first arc undergoes a transition from large to small. The VAEGAN network allows for the utilization of a latent variable to describe the aging condition of Li-ion batteries, encompassing factors such as loss of lithium inventory and loss of active material, through the analysis of the EIS data collected during the capacity decline of the batteries.

4.3. Capacity estimation

In this subsection, we utilize two sets of meaningful latent variables extracted by VAEGAN from EIS data as inputs to GPR in order to achieve capacity estimation. It is also compared with the following three methods. Method I is similar to the one mentioned by Zhang [14], which uses the raw EIS data as an input to the GPR in order to directly predict the capacity. This method is referred to as RawEIS in this paper. Method 2, similar to the one mentioned by Obregon [23], uses CAE to extract features from the EIS data. These features are then used as input to the GPR for capacity prediction. Method 3: Eliminate the discriminator in VAEGAN, that is, use a VAE to extract latent variables from the EIS data and use them as inputs to the GPR for capacity prediction. Except for the implementation of the first method, the neural network complexity of the remaining methods is designed to be as similar as possible to the VAEGAN proposed in this paper, in order to facilitate accurate comparisons.

Fig. 7 displays the results of the capacity estimation of the PJ121 using the four different methods, compared to the true values. The results of the evaluation of the remaining cells are shown in Fig. S1. As shown in the figure, the RawEIS method displays a notable discrepancy between the predicted and actual values for all cells. Conversely, both the VAE-based and VAEGAN-based methods demonstrate predicted values that closely align with the actual values for all cells. Fig. 8 displays the four methods for estimating the variability of PJ121 capacity with cycling, while Fig. S2 shows the results of the remaining cells. While the confidence intervals for the predictions are the smallest among the four methods, the Raw EIS method is not suitable for predicting the residual capacity of unbalanced-use Li-ion batteries, especially when the residual capacity is low. The predicted values show unpredictable and significant drifts. The performance of CAE-based methodologies in predicting battery capacity varies among different batteries. PJ124 and PJ125 show closer predicted capacity values to the actual value, while the other cases of battery capacity prediction indicate a high level of both small and large bias. Comparatively, the methods based on VAE and VAEGAN demonstrate better prediction performance for the degradation processes of Li-ion battery capacity. The distinction between them is that the latter predicts a slightly smaller confidence interval than the former.

Table 1 displays the results obtained from estimating the capacity of each cell. The VAEGAN-based method's predictive accuracy remains consistent across different cells. Its capacity prediction for Li-ion batteries under uneven usage stands out compared to other methods, with

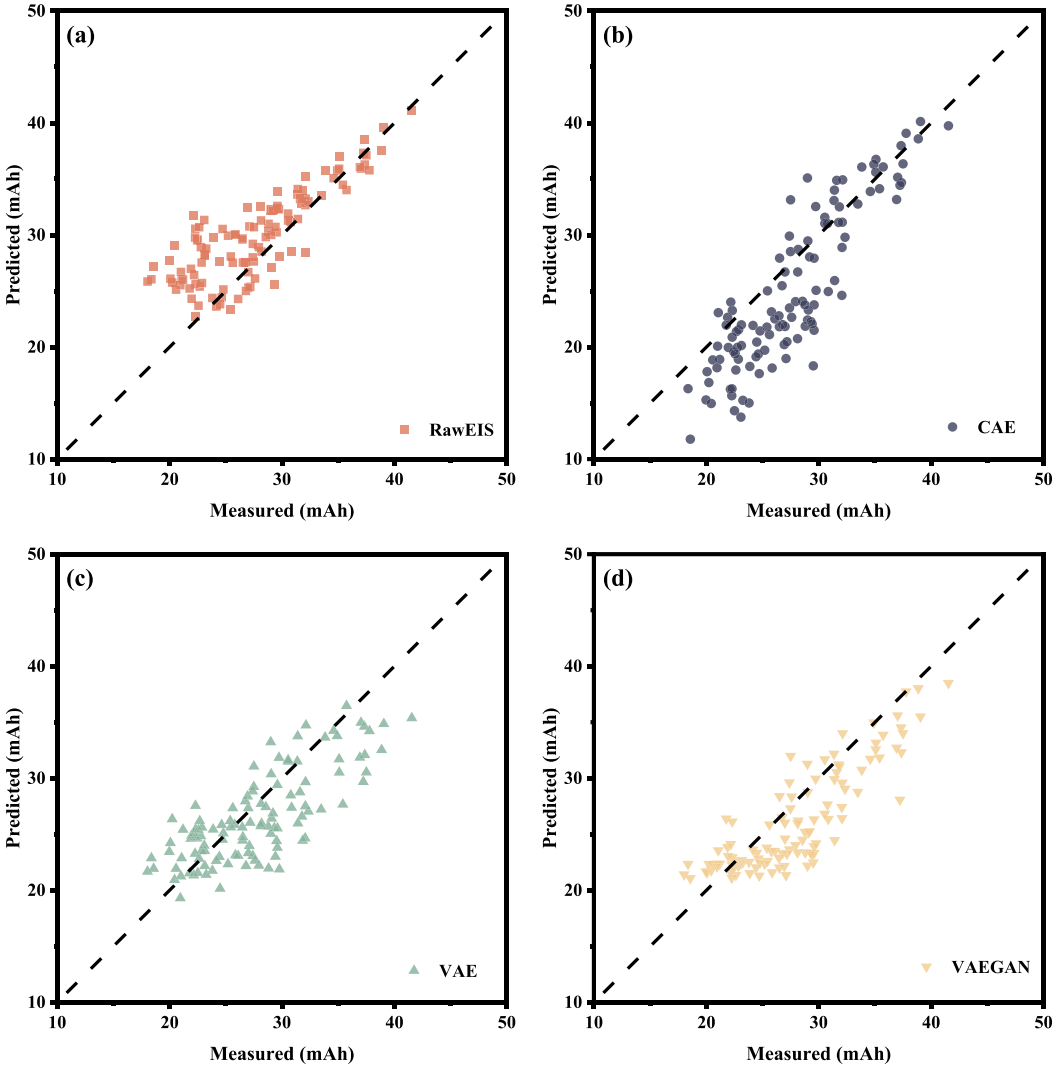

Fig. 7. Predicted capacity with respect to the measured capacity of PJ121 using four methods. (a) RawEIS, (b) CAE-based, (c) VAE-based, (d) VAEGAN-based.

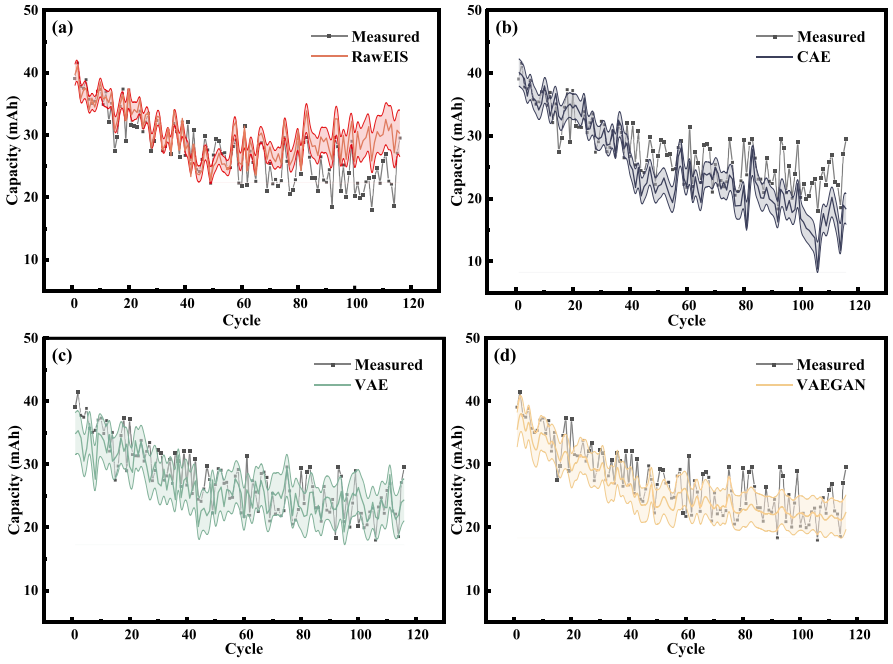

Fig. 8. Capacity estimations for PJ121 using different methods. (a) RawEIS, (b) CAE-based, (c) VAE-based, (d) VAEGAN-based. The shaded region indicates a standard deviation of ±1.

Table 1
Capacity estimations for all testing data using different features as input for GPR.

Evaluation metrics	Methods	Cell						Average
		PJ121	PJ122	PJ123	PJ124	PJ125	PJ126	
RMSE (mAh)	RawEIS	3.779	8.091	13.658	4.745	5.256	7.248	7.129
	CAE	4.383	4.570	3.682	3.032	3.550	4.278	3.916
	VAE	3.539	2.924	3.228	3.265	3.542	2.920	3.236
	VAEGAN	**3.215**	**2.899**	**3.197**	**2.654**	**3.063**	**2.436**	**2.911**
MAE (mAh)	RawEIS	2.962	6.921	11.908	4.341	4.653	6.518	6.217
	CAE	3.587	3.780	3.038	2.568	2.825	3.708	3.251
	VAE	2.880	2.401	2.536	2.661	2.799	2.285	2.594
	VAEGAN	**2.587**	**2.342**	**2.529**	**2.233**	**2.484**	**2.074**	**2.375**

an RMSE of 2.911 mAh and an MAE of 2.375 mAh.

4.4. Robustness evaluation

VAEGAN is insensitive to noise in the input data for two reasons. Firstly, the encoder of VAEGAN can map the noisy input samples to a low-dimensional latent space. Secondly, the discriminator of VAEGAN can provide a more reasonable reconstructed loss function instead of simply relying on pixel-level errors [39]. This will not affect the expressiveness of the latent variables, even if the input samples contain noise. The noise robustness of the method proposed in this paper is examined in comparison to the other three methods in this subsection.

The EIS data of the original test samples are perturbed with Gaussian noise with a mean of 0 and a variance of σ^2. In order to investigate the robustness of the method for predicting the capacity of Li-ion batteries, we used the latent variables extracted from the noisy EIS through

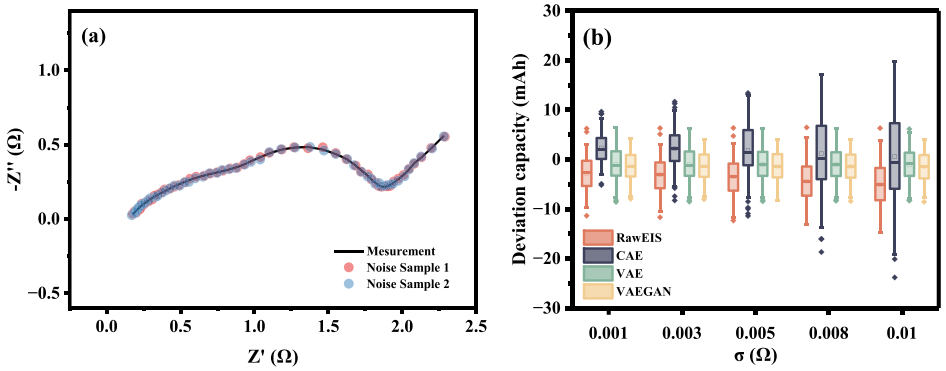

Fig. 9. (a) EIS samples with Gaussian noise having a standard deviation (σ) of 0.005. (b) Statistics on the bias of the PJ121 per-cycle residual capacity prediction using four different methods with input data containing various noise levels.

VAEGAN as the input for GPR. The perturbed EIS curves can be expressed as follows:

$$Z' = Z + \Delta Z, \text{ where } \Delta Z \sim N(0, \sigma^2) \quad (20)$$

Test samples with different levels of noise were generated by adding Gaussian noise with σ of 0.001, 0.003, 0.005, 0.008, and 0.01. Fig. 9(a) depicts two EIS samples with a noise level (σ) of 0.005. The data from the 80th cycle of PJ121 was selected, and 100 samples containing noise were generated using the above method. These samples were predicted using each of the four methods, and the results are shown in Fig. 10. Additional EIS samples and predictions for different noise level cases are shown in Fig. S3 and S4. Upon inspecting the graph, it becomes clear that the RawEIS and CAE-based methods exhibit stable predictive capability when noise levels are relatively low. However, as noise levels gradually increase, both methods exhibit significant fluctuations. Meanwhile, the VAE or VAEGAN-based approaches continue to demonstrate consistent prediction performance at this level of noise.

Fig. 9(b) clearly illustrates the overall prediction performance of each method at various noise levels. The boxplot in Fig. 9(b) illustrates the prediction bias statistics of the different methods for estimating the capacity of all cycle counts of PJ121 at various noise levels of the input data. The results for the other numbered cells are shown in Fig. S5. The whiskers extend to the most extreme data points that are not considered outliers, and the outliers are represented as independent "◆" symbols in the box plot. The center line indicates the median and the edges of the box represent the 25th and 75th percentiles. As expected, the noise robustness of the CAE-based method is even worse than that of the RawEIS method because the extracted features are discrete and difficult to interpret. Both VAE and VAEGAN neural networks utilize convolutional layers, enabling the neural network to concentrate on the input data as a whole, rather than the magnitude of individual data point values. This feature brings about noise reduction. At the same time, they both utilize variational inference techniques, enabling them to evaluate the likelihood that the input data aligns with a specific scenario from a probabilistic perspective. These two methods, although they introduce some uncertainty in the prediction process, are more resistant to data feature extraction than CAE, which is a point-to-point coding method, especially in cases where noise is present. The VAEGAN's discriminator enhances its learning capability and makes the data feature extraction more robust, thereby reducing uncertainty in the prediction process. As a result, the VAEGAN-based method maintains high prediction accuracy and strong noise resistance.

5. Conclusion

In this research, a method based on VAEGAN is proposed for analyzing EIS data obtained from Li-ion batteries. The method aims to identify latent variables that correspond to the level of battery aging as reflected in the EIS measurements. By examining the latent variables, it has been determined that the magnitude of these variables can somewhat indicate the level of aging in Li-ion batteries during their usage. Through the extraction of latent variables from EIS data by the model, accurate capacity estimation during the aging process of Li-ion batteries is achievable, even in cases of uneven battery utilization. Comparative analysis reveals that the proposed method reduces prediction errors by 59.2 %, 25.7 %, and 10.0 % in comparison to RawEIS, CAE, and VAE-based methods, respectively. The RMSE and MAE for the method proposed in this paper to estimate the capacity of Li-ion batteries are 2.911mAh and 2.375mAh, respectively. The robustness of the extracted latent variables against data noise is attributed to the encoder's dimensionality reduction capability and the discriminator's ability to enhance loss reconstruction accuracy. Consequently, the method demonstrates resilience to noise in EIS data, enhancing its suitability for practical applications. Unlike manual feature extraction methods from EIS data that rely on domain experts' prior knowledge, the unsupervised deep learning approach of dimensionality reduction using VAEGAN is better suited for handling large datasets. The study focuses on utilizing VAEGAN's feature downscaling function to extract EIS data features for estimating lithium-ion battery capacity under uneven usage conditions. Future research directions include leveraging VAEGAN's data generation capabilities to expand datasets and establish connections between VAEGAN's encoder and other neural networks, enabling more precise prediction of aging state parameters associated with Li-ion batteries.

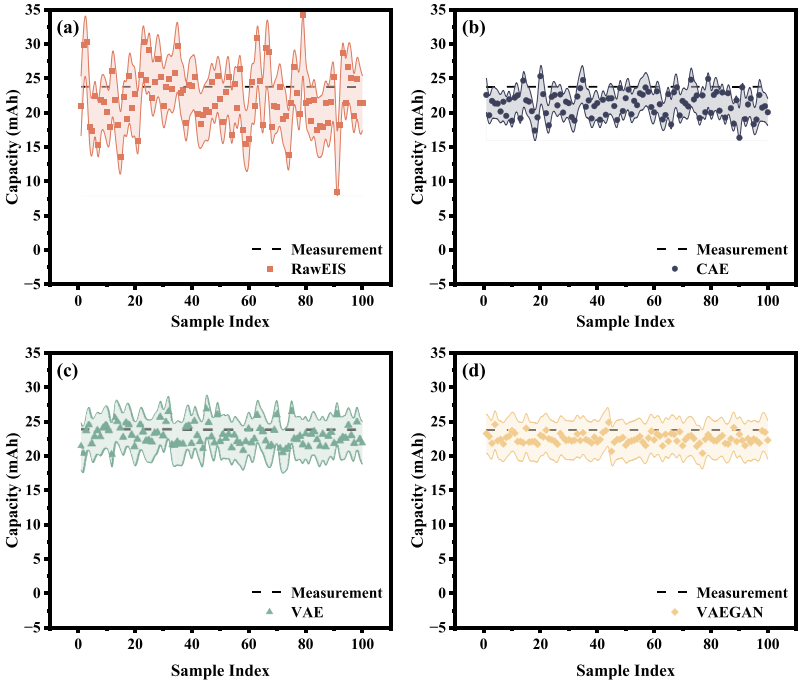

Fig. 10. Prediction results for four methods on 100 samples with Gaussian noise, with a standard deviation of 0.005. (a) RawEIS, (b) CAE-based, (c) VAE-based, (d) VAEGAN-based. The shaded region indicates a standard deviation of ±1.

CRediT authorship contribution statement

Jianying Yuan: Writing – original draft, Methodology, Conceptualization. **Jie Zhao:** Supervision, Resources, Funding acquisition. **Yaoguang Yu:** Writing – review & editing, Methodology. **Qingze Han:** Writing – review & editing, Supervision. **Guofeng Cui:** Methodology, Funding acquisition, Conceptualization.

Declaration of competing interest

The authors declare that they have no known competing financial interests or personal relationships that could have appeared to influence the work reported in this paper.

Data availability

Data will be made available on request.

Acknowledgments

This research was funded by the National Natural Science Foundation of China, Grant number 51571093, 51271205.

Supplementary materials

Supplementary material associated with this article can be found, in the online version, at doi:10.1016/j.electacta.2024.144694.

References

[1] Y. Zhang, H. Liu, Z. Xie, W. Qu, D.J. Freschi, J. Liu, Progress and perspectives of lithium aluminum germanium phosphate-based solid electrolytes for lithium batteries, Adv. Funct. Mater. 33 (2023) 2300973, https://doi.org/10.1002/ADFM.202300973.
[2] S. Zhu, J. Ni, The critical role of carbon nanotubes in bridging academic research to commercialization of lithium batteries, Chem. Rec. 22 (10) (2022) e202200125, https://doi.org/10.1002/TCR.202200125.
[3] H. Jia, W. Xu, Electrolytes for high-voltage lithium batteries, Trends Chem. 4 (7) (2022) 627–642, https://doi.org/10.1016/J.TRECHM.2022.04.010.
[4] P. Iurilli, C. Brivio, V. Wood, On the use of electrochemical impedance spectroscopy to characterize and model the aging phenomena of lithium-ion batteries: a critical review, J. Power Sources 505 (2021) 229860, https://doi.org/10.1016/j.jpowsour.2021.229860.
[5] W. Hu, Y. Peng, Y. Wei, Y. Yang, Application of electrochemical impedance spectroscopy to degradation and aging research of lithium-ion batteries, J. Phys. Chem. C 127 (9) (2023) 4465–4495, https://doi.org/10.1021/acs.jpcc.3c00033.
[6] C.R. Birkl, M.R. Roberts, E. McTurk, P.G. Bruce, D.A. Howey, Degradation diagnostics for lithium ion cells, J. Power Sources 341 (2017) 373–386, https://doi.org/10.1016/j.jpowsour.2016.12.011.
[7] B. Su, X. Ke, C. Yuan, Modeling the effects of state of charge and temperature on calendar capacity loss of nickel-manganese-cobalt lithium-ion batteries, J. Energy Storage 49 (2022) 104105, https://doi.org/10.1016/J.EST.2022.104105.
[8] Y. Zhang, Y.F. Li, Prognostics and health management of Lithium-ion battery using deep learning methods: a review, Renew. Sustain. Energy Rev. 161 (2022) 112282, https://doi.org/10.1016/J.RSER.2022.112282.
[9] K. Luo, X. Chen, H. Zheng, Z. Shi, A review of deep learning approach to predicting the state of health and state of charge of lithium-ion batteries, J. Energy Chem. 74 (2022) 159–173, https://doi.org/10.1016/j.jechem.2022.06.049.
[10] J. Zhao, X. Feng, Q. Pang, J. Wang, Y. Lian, M. Ouyang, et al., Battery prognostics and health management from a machine learning perspective, J. Power Sources 581 (2023) 233474, https://doi.org/10.1016/j.jpowsour.2023.233474.
[11] K. Mc Carthy, H. Gullapalli, K.M. Ryan, T. Kennedy, Use of impedance spectroscopy for the estimation of Li-ion battery state of charge, state of health and internal temperature, J. Electrochem. Soc. 168 (8) (2021) 080517, https://doi.org/10.1149/1945-7111/ac1a85.
[12] N. Meddings, M. Heinrich, F. Overney, J.S. Lee, V. Ruiz, E. Napolitano, et al., Application of electrochemical impedance spectroscopy to commercial Li-ion cells: a review, J. Power Sources 480 (2020) 228742, https://doi.org/10.1016/j.jpowsour.2020.228742.
[13] R. Tatara, P. Karayaylali, Y. Yu, Y. Zhang, L. Giordano, F. Maglia, et al., The Effect of electrode-electrolyte interface on the electrochemical impedance spectra for positive electrode in Li-Ion battery, J. Electrochem Soc. 166 (3) (2019) A5090–A5098, https://doi.org/10.1149/2.0121903JES/XML.
[14] Y. Zhang, Q. Tang, Y. Zhang, J. Wang, U. Stimming, A.A. Lee, Identifying degradation patterns of lithium ion batteries from impedance spectroscopy using machine learning, Nat. Commun. 11 (1) (2020) 1706, https://doi.org/10.1038/s41467-020-15235-7.
[15] J. Zhu, Q. Zhang, L. Mereacre, X. Wang, B. Jiang, H. Dai, et al., Alternating current impedance probing capacity of lithium-ion battery by gaussian process regression, Energy Technol. 10 (8) (2022) 2200437, https://doi.org/10.1002/ente.202200437.
[16] K. Luo, H. Zheng, Z. Shi, A simple feature extraction method for estimating the whole life cycle state of health of lithium-ion batteries using transformer-based neural network, J. Power Sources 576 (2023) 233139, https://doi.org/10.1016/j.jpowsour.2023.233139.
[17] B. Jiang, J. Zhu, X. Wang, X. Wei, W. Shang, H. Dai, A comparative study of different features extracted from electrochemical impedance spectroscopy in state of health estimation for lithium-ion batteries, Appl. Energy 322 (2022) 119502, https://doi.org/10.1016/j.apenergy.2022.119502.
[18] X. Wang, X. Wei, H. Dai, Estimation of state of health of lithium-ion batteries based on charge transfer resistance considering different temperature and state of charge, J. Energy Storage 21 (2019) 618–631, https://doi.org/10.1016/j.est.2018.11.020.
[19] R. He, Y. He, W. Xie, B. Guo, S. Yang, Comparative analysis for commercial li-ion batteries degradation using the distribution of relaxation time method based on electrochemical impedance spectroscopy, Energy 263 (2023) 125972, https://doi.org/10.1016/J.ENERGY.2022.125972.
[20] H.S. Chan, E.J.F. Dickinson, T.P. Heins, J. Park, M. Gaberšček, Y.Y. Lee, et al., Comparison of methodologies to estimate state-of-health of commercial Li-ion cells from electrochemical frequency response data, J. Power Sources 542 (2022) 231814, https://doi.org/10.1016/j.jpowsour.2022.231814.
[21] Y. Zhu, B. Jiang, J. Zhu, X. Wang, R. Wang, X. Wei, et al., Adaptive state of health estimation for lithium-ion batteries using impedance-based timescale information and ensemble learning, Energy 284 (2023) 129283, https://doi.org/10.1016/J.ENERGY.2023.129283.
[22] Y. Zhou, G. Dong, Q. Tan, X. Han, C. Chen, J Wei, State of health estimation for lithium-ion batteries using geometric impedance spectrum features and recurrent Gaussian process regression, Energy 262 (2023) 125514, https://doi.org/10.1016/j.energy.2022.125514.
[23] J. Obregon, Y.R. Han, C.W. Ho, D. Mouraliraman, C.W. Lee, J.Y. Jung, Convolutional autoencoder-based SOH estimation of lithium-ion batteries using electrochemical impedance spectroscopy, J. Energy Storage 60 (2023) 106680, https://doi.org/10.1016/j.est.2023.106680.
[24] R. Xiong, J. Tian, W. Shen, J. Lu, F. Sun, Semi-supervised estimation of capacity degradation for lithium ion batteries with electrochemical impedance spectroscopy, J. Energy Chem. 76 (2023) 404–413, https://doi.org/10.1016/j.jechem.2022.09.045.
[25] S. Kim, Y.Y. Choi, J.I. Choi, Impedance-based capacity estimation for lithium-ion batteries using generative adversarial network, Appl. Energy 308 (2022) 118317, https://doi.org/10.1016/j.apenergy.2021.118317.
[26] P.K. Jones, U. Stimming, A.A. Lee, Impedance-based forecasting of lithium-ion battery performance amid uneven usage, Nat Commun 13 (1) (2022) 4806, https://doi.org/10.1038/s41467-022-32422-w.
[27] C. Zhang, J. Butepage, H. Kjellstrom, S. Mandt, Advances in variational inference, IEEE Trans. Pattern Anal. Mach. Intell. 41 (8) (2019) 2008–2026, https://doi.org/10.1109/TPAMI.2018.2889774.
[28] Rasmussen C.E. Gaussian processes in machine learning. In: Bousquet O., von Luxburg U., Rätsch G. (eds) Advanced Lectures on Machine Learning. ML 2003. Lecture Notes in Computer Science 2004:63–71. doi:10.1007/978-3-540-28650-9_4.
[29] K.S. Sudeep, K.K. Pal, Preprocessing for image classification by convolutional neural networks, in: Proceedings of the 2016 IEEE International Conference on Recent Trends in Electronics, Information and Communication Technology, RTEICT 2016 - Proceedings, 2016, pp. 1778–1781, https://doi.org/10.1109/RTEICT.2016.7808140.
[30] Q. Gong, P. Wang, Z. Cheng, An encoder-decoder model based on deep learning for state of health estimation of lithium-ion battery, J. Energy Storage 46 (2022) 103804, https://doi.org/10.1016/j.est.2021.103804.
[31] C. Nkikabahizi, W. Cheruiyot, A. Kibe, Chaining Zscore and feature scaling methods to improve neural networks for classification, Appl. Soft Comput. 123 (2022) 108908, https://doi.org/10.24433/CO.6303.
[32] T. Jiang, J. Cheng, Target recognition based on CNN with LeakyReLU and PReLU activation functions, in: Proceedings of the 2019 International Conference on Sensing, Diagnostics, Prognostics, and Control, SDPC 2019, 2019, pp. 718–722, https://doi.org/10.1109/SDPC.2019.00136.
[33] R. Edward, N. Hannes, Gaussian Processes for Machine Learning (GPML) Toolbox, J. Mach. Learn. Res. 11 (2010) 3011–3015, https://doi.org/10.5555/1756006.1953029.
[34] A. Maheshwari, M. Heck, M. Santarelli, Cycle aging studies of lithium nickel manganese cobalt oxide-based batteries using electrochemical impedance spectroscopy, Electrochim. Acta 273 (2018) 335–348, https://doi.org/10.1016/J.ELECTACTA.2018.04.045.
[35] D. Andre, M. Meiler, K. Steiner, H. Walz, T. Soczka-Guth, D.U. Sauer, Characterization of high-power lithium-ion batteries by electrochemical impedance spectroscopy. II: modelling, J. Power Sources 196 (2011) 5349–5356, https://doi.org/10.1016/j.jpowsour.2010.07.071.
[36] C. Pastor-Fernández, K. Uddin, G.H. Chouchelamane, W.D. Widanage, J. Marco, A comparison between electrochemical impedance spectroscopy and incremental capacity-differential voltage as Li-ion diagnostic techniques to identify and quantify the effects of degradation modes within battery management systems, J. Power Sources 360 (2017) 301–318, https://doi.org/10.1016/j.jpowsour.2017.03.042.

[37] E. Teliz, C.F. Zinola, V. Díaz, Identification and quantification of ageing mechanisms in Li-ion batteries by Electrochemical impedance spectroscopy, Electrochim. Acta 426 (2022) 140801, https://doi.org/10.1016/j.electacta.2022.140801.
[38] R. Xiong, Y. Pan, W. Shen, H. Li, F. Sun, Lithium-ion battery aging mechanisms and diagnosis method for automotive applications: recent advances and perspectives, Renew. Sustain. Energy Rev. 131 (2020) 110048, https://doi.org/10.1016/J.RSER.2020.110048.
[39] X. Hou, K. Sun, L. Shen, G. Qiu, Improving variational autoencoder with deep feature consistent and generative adversarial training, Neurocomputing 341 (2019) 183–194, https://doi.org/10.1016/J.NEUCOM.2019.03.013.